High-Spin Rotational Structures in ^{76}Kr

J.J. Valiente-Dobón,[1, *] C.E. Svensson,[1, †] C.D. O'Leary,[2, ‡] I. Ragnarsson,[3] C. Andreoiu,[1, 4] D.E. Appelbe,[5]
R.A.E. Austin,[6] G.C. Ball,[7] J.A. Cameron,[6] M.P. Carpenter,[8] R.M. Clark,[9] M. Cromaz,[9] D. Dashdorj,[10]
P. Fallon,[9] P. Finlay,[1] S.J. Freeman,[8] P.E. Garrett,[1, 7] A. Görgen, G.F. Grinyer,[1] D.F. Hodgson,[7]
B. Hyland,[1] D. Jenkins,[2] F. Johnston-Theasby,[2] P. Joshi,[2] N.S. Kelsall,[2] A.O. Macchiavelli,[9]
F. Moore,[8] G. Mukherjee,[8] A.A. Phillips,[1] W. Reviol,[12] D. Sarantites,[12] M.A. Schumaker,[1]
D. Seweryniak,[8] M.B. Smith,[7] J.C. Waddington,[6] R. Wadsworth,[2] D. Ward,[9] and S.J. Williams[13]

[1]*Department of Physics, University of Guelph, Guelph, Ontario N1G 2W1, Canada*
[2]*Department of Physics, University of York, Heslington, York YO10 5DD, UK*
[3]*Department of Physics, Lund Institute of Technology, P.O. Box 118 S-221 00 Lund, Sweden*
[4]*Oliver Lodge Laboratory, University of Liverpool, Liverpool L69 3BX, UK*
[5]*CLRC Daresbury Laboratory, Daresbury, Warrington WA4 4AD, UK*
[6]*Department of Physics and Astronomy, McMaster University, Hamilton, Ontario L8S 4K1, Canada*
[7]*TRIUMF, 4004 Wesbrook Mall, Vancouver, British Columbia, V6T 2A3, Canada*
[8]*Physics Division, Argonne National Laboratory, Argonne, Illinois 60439*
[9]*Lawrence Berkeley National Laboratory, Berkeley, California 94720*
[10]*North Carolina State University, Raleigh, North Carolina 27695*
[11]*CEA Saclay, DAPNIA/SPhN, 91191 Gif-sur-Yvette Cedex, France*
[12]*Department of Chemistry, Washington University, St. Louis MO 63130*
[13]*Department of Physics, University of Surrey, Guildford GU2 7XH, UK*
(Dated: January 7, 2005)

High-spin states in $^{76}_{36}$Kr$_{40}$ have been populated in the ^{40}Ca(^{40}Ca,4p)^{76}Kr fusion-evaporation reaction at a beam energy of 165 MeV, and studied using the GAMMASPHERE and MICROBALL multi-detector arrays. The ground-state band and two signature-split negative parity bands of ^{76}Kr have been extended to ∼30$\hbar$. Lifetime measurements using the Doppler-shift attenuation method show that the transition quadrupole moment of these three bands decrease as they approach their maximum-spin states. Two signatures of a new rotational structure with remarkably rigid rotational behavior have been identified. The high-spin properties of these rotational bands are analyzed within the framework of configuration-dependent cranked Nilsson-Strutinsky calculations.

I. INTRODUCTION

The proton-rich nucleus $^{76}_{36}$Kr$_{40}$ has long been known to possess large deformations near its ground state [1]. Numerous theoretical calculations [2, 3, 4, 5] suggest a highly-deformed near-prolate shape for the ground state of this nucleus, with an oblate minimum located approximately 600 keV higher in energy. Indeed, lifetime measurements [5] for the low-spin states of the positive-parity ground-state band have shown that the nucleus supports a quadrupole deformation of $|\beta_2|{\approx}0.33$ (under the assumption of an axial symmetric shape). This band has previously been observed to 24$\hbar$ [5], with the sharp upbend in its moment of inertia at a rotational frequency ω=0.65 MeV/$\hbar$ attributed to an effectively simultaneous rotational alignment of $g_{9/2}$ protons and neutrons.

The favoured negative-parity excited band (in the following pages we will refer to this band as Band **D**) observed in ^{76}Kr [5, 6, 7] has been assigned to the

* Electronic address: valiente@physics.uoguelph.ca
† Electronic address: sven@physics.uoguelph.ca
‡ Electronic address: christopher.oleary@physics.org

two-quasiproton configuration based on the $\pi[431]\frac{3}{2}^+ \otimes \pi[312]\frac{3}{2}^-$ Nilsson orbitals [5]. This negative-parity sequence has been observed to exhibit very large $B(E2)$ strengths [6]. Together with large values for, and a strong similarity between, its measured kinematic ($\Im^{(1)}$) and dynamic ($\Im^{(2)}$) moments of inertia, these observations have led to the inference that this structure is among the best examples of rigid, collective rotation in the $A{\sim}70$–80 mass region. This rigid rotation has been attributed to the strong suppression of static pairing correlations resulting from the combined effects of the low level density close to the large N, Z=38 shell gap at $\beta_2{\approx}0.35$, and the blocking of the key $[431]\frac{3}{2}^+$ and $[312]\frac{3}{2}^-$ proton orbitals below this gap in the favoured negative-parity configuration [5, 7]. The neutron alignment in this negative-parity band occurs at a rotational frequency ω=0.75 MeV/$\hbar$, approximately 0.1 MeV/$\hbar$ higher than in the ground-state band, suggesting a small change in equilibrium deformation or residual neutron-proton interactions for this excited configuration [5, 7].

Recent work has established another signature-split negative-parity structure (in the following pages we will refer to this band as Band **E**) in ^{76}Kr to 13$\hbar$ [8], with the onset of a rotational alignment observed at ω=0.55 MeV/$\hbar$. A detailed study of the properties of this

band led to its assignment to a two-quasineutron config-uration based on the $\nu[301]\frac{3}{2}^- \otimes \nu[422]\frac{5}{2}^+$ Nilsson orbitals, with the alignment attributed to $g_{9/2}$ protons [8]. The same data also allowed the observation of a strongly-coupled, $\Delta I=1$ band in ^{76}Kr to 10^+ [9]. This latter structure was assigned to a two-quasineutron configuration based on a $K^\pi = 4^+$ coupling of the $\nu[301]\frac{3}{2}^- \otimes \nu[303]\frac{5}{2}^-$ Nilsson orbitals at a prolate deformation of $\beta_2 \approx 0.34$.

Lifetimes of the low-spin states in the ground-state band for ^{76}Kr have been previously studied up to spin 10^+ [5, 6, 10]. According to Gross *et al.* [5] the transition quadrupole moment, before the pair breaking, changes from 2.90 *eb* for the 425 keV transition to 2.53 *eb* for the 1189 keV transition, which corresponds to an approximately constant quadrupole deformation for this spin range $|\beta_2|\approx0.33$, if a prolate axial symmetric shape is considered. A few lifetimes for the low-spin transitions in the negative-parity yrast band have been reported by Piercey *et al.* [6]. Nevertheless these lifetimes have to be treated carefully, since the detector resolution in this experiment did not provide sufficiently clear Doppler profiles.

The present article reports on the extension to higher angular momenta of all of the previously observed bands in ^{76}Kr and the identification of a new high-spin band with remarkably rigid rotational behavior. The lifetimes of the high-spin states of the ground-state band and the two signature-split negative-parity yrast bands have been measured using the Doppler shift attenuation method [11]. These bands present a substantial loss of collectivity as they approach the highest-spin states. The properties of all bands observed to high angular momenta are compared with configuration-dependent cranked Nilsson-Strutinsky (CNS) calculations without pairing [12, 13]. These calculations provide a good description of the observed high-spin behavior, and lead to configuration assignments characterized by the number of $g_{9/2}$ proton and neutron orbitals occupied at high angular momentum in each band.

II. EXPERIMENT

High-spin states in ^{76}Kr were populated via the ^{40}Ca(^{40}Ca,4p)^{76}Kr reaction. A 165-MeV ^{40}Ca beam was provided by the ATLAS accelerator at Argonne National Laboratory. A thin- and a backed-target experiment were performed. The thin target was 350 μg/cm^2 ^{40}Ca sandwiched between two 150 μg/cm^2 Au layers to prevent oxidation during installation of the target in the vacuum chamber. The backed target was a 225 μg/cm^2 ^{40}Ca layer evaporated onto a 13.9 mg/cm^2 Au backing. Gamma rays were detected with 99 Compton-suppressed HPGe detectors of the GAMMASPHERE array [14], in coincidence with charged particles detected and identified with the 95-element CsI(Tl) MICROBALL detector [15]. The beam current was maintained at approximately 2.3 particle-nA, and a total of 1.5×10^9 and 4.5×10^8 particle–γ co-
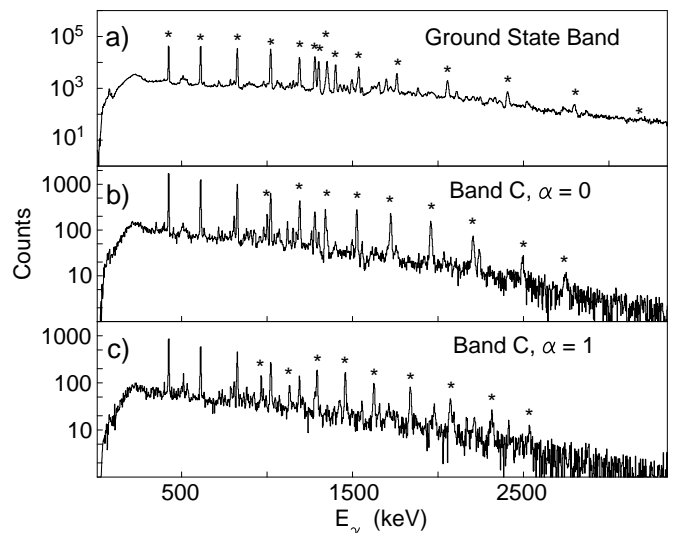

FIG. 1: Gamma-ray spectra obtained by summing pairs of double coincidence gates set on in-band transitions in a) the ground-state band of ^{76}Kr, b) the α=0 signature of Band **C**, and c) the α=1 signature of Band **C**. In each case, the in-band transitions are denoted by *.

incidence events were recorded on magnetic tape during an 83- and 24-hour thin- and backed-target experiment, respectively. The hardware trigger required at least four HPGe detectors (after Compton suppression) to fire in prompt coincidence in each experiment.

Gamma rays emitted in the decay of excited states of ^{76}Kr were isolated in the offline analysis by selecting events in which four protons were detected in prompt coincidence in the MICROBALL. Events in which five protons (populating ^{75}Br), an alpha-particle and four protons (^{72}Se), or four protons and a neutron (^{75}Kr), were evaporated but one particle escaped detection were removed from this data set by further requiring the sum of the kinetic energies of the protons and the total γ-ray energy detected in the GAMMASPHERE to be consistent with the Q-value for the four-proton evaporation channel [16]. The selected events were unfolded into a three-dimensional γ–γ–γ coincidence cube in which the γ-ray energies were Doppler-shift corrected on an event-by-event basis according to the momentum vectors of the detected protons [17]. The Radware suite of programs [18] was used to analyze this coincidence cube and establish γ-ray coincidence relationships and the ^{76}Kr decay scheme. With the same channel selection criteria, an asymmetric two-dimensional DCO (directional correlations from oriented states) matrix was also constructed. Gamma rays detected at angles between 79.2° and 100.8° relative to the beam axis were incremented on the x axis of this matrix, while those detected at angles >142.6° were incremented on the y axis. As described in, for example, Ref. [19] the ratio of the intensities of the coincidence peaks at locations (γ_1, γ_2) and (γ_2, γ_1) in this matrix, $R_{\rm DCO} = I(\gamma_1,\gamma_2)/I(\gamma_2,\gamma_1)$, provides useful information about transition multipolarities. In particu-
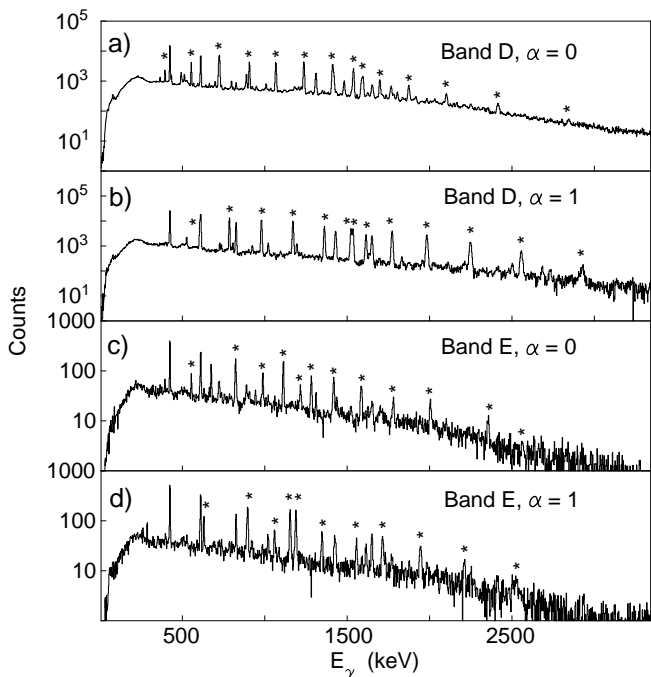
FIG. 2: Gamma-ray spectra obtained by summing pairs of double coincidence gates set on in-band transitions in a) the $\alpha=0$ signature of Band **D**, b) the $\alpha=1$ signature of Band **D**, c) the $\alpha=0$ signature of Band **E**, and d) the $\alpha=1$ signature of Band **E**. In each case, the in-band transitions are denoted by *.

lar, taking a known stretched quadrupole transition for γ_1 yielded R_{DCO} values of ≈ 1.0 and ≈ 0.55 when γ_2 was a stretched quadrupole or stretched dipole transition, respectively.

The thin-target data allowed the extraction of the lifetimes from the states at the top of the rotational bands, where lifetimes are of the order of tens of femtoseconds. These states decay while the recoil ions are slowing down inside the thin ^{40}Ca target. The centroid-shift Doppler attenuation method [11], was used to measure the lifetimes of the high-spin states ($I \gtrsim 18\hbar$) in the most strongly populated bands in ^{76}Kr. In the analysis, the γ rays were Doppler corrected for a recoil velocity, β_0, that corresponds to the velocity when the recoil was formed, as calculated according to the kinematics of the reaction. This Doppler-corrected data was sorted into 16 matrices, one for each of the 16 rings of GAMMASPHERE, requiring the coincidence between the detectors in one specific ring and any other detector. Each of the spectra for the different rings show that the γ-ray peaks are slightly shifted. The shift in the centroids of the γ-ray peaks shows that the γ-ray transitions were emitted while the recoil was slowing down within the target. The mean instantaneous recoil velocity β_t for each transition can be obtained measuring the centroid shifts of the peaks and the ratio $F(\tau) = \beta_t/\beta_0$, can be defined. The stopping powers were obtained using the SRIM-2003 code [20]. The fitting program takes into account the initial momenta of

^{76}Kr recoil, so no bias is introduced in the fit procedure due to the angular dependence in the particle detection efficiency of MICROBALL. While a bias is introduced in the momentum distribution of the recoils by MICROBALL due to the particle-detection angular dependence, it is important when α particles are involved [21, 22], and it was found to be negligible in the case of protons [23].

The backed-target data provided additional lifetime information for the lower-spin states. Five matrices similar to the thin-target data were produced, in this case the required angles to produce the matrices were 31.7°, 37.4°, 90.0°, 142.6° and 148.3°. The program LINESHAPE [24] was used to calculate velocity distributions and fit the line shapes. The program LINESHAPE can only perform calculations at three angles: one at forward angles, one at 90.0° and another at backward angles. In order to increase the statistics at the forward and backward angles, weighted averages of the 31.7°, 37.4° and 142.6°, 148.3° angles were used. To simulate the slowing down process the Ziegler and Chu stopping powers [25] were used. The velocity distribution seen by the forward- and backward-angle detectors as a function of time was calculated from 10,000 histories. The side feeding intensities were extracted from the spectra generated at 90.0°. The program was modified to take into account the initial momenta of ^{76}Kr recoil resulting from the particle evaporation.

III. RESULTS

Gamma-ray coincidence spectra for each of the high-spin bands in ^{76}Kr, obtained by summing all pairs of clean double coincidence gates set on in-band transitions, are shown in Figs. 1 and 2, while the decay scheme deduced for ^{76}Kr from the present work is shown in Fig. 3. The bands are labelled from **A** to **E**, in addition to the ground-state band, in Fig. 3. These labels will be used to refer to the bands throughout the remainder of this paper. Tables I–VI summarize the measured data for each band.

The ground-state band of ^{76}Kr had been observed to $24\hbar$ in previous studies [5]. We have extended this structure to $(30\hbar)$ through the observation of 2406, 2793 and 3207-keV transitions. As discussed in the next section, the (30^+) state represents the effective termination of this rotational band.

Band **A** is the strongly-coupled band first identified by Döring *et al.* [9] and tentatively established to 10^+. The current data allows an extension of this structure to 16^+. This band was tentatively assigned positive parity by Döring *et al.* [9]. The DCO measurements presented here for the ten transitions linking this band to the remainder of the ^{76}Kr decay scheme confirm this assignment. We note that, due to the lack of clean gates among the in-band quadrupole transitions, the DCO ratios for Band **A** presented in Table II were obtained with gates on the strong $\Delta I=1$ cross-over transitions at low

Band D

Band C

Band B

Band A

Band E

^{76}Kr

FIG. 3: Level scheme derived from the present data set. Gamma-ray transition energies are given to the nearest keV and arrow widths are proportional to relative γ-ray intensities. Levels are grouped into five bands, labelled **A** to **E**, in addition to the ground-state band.
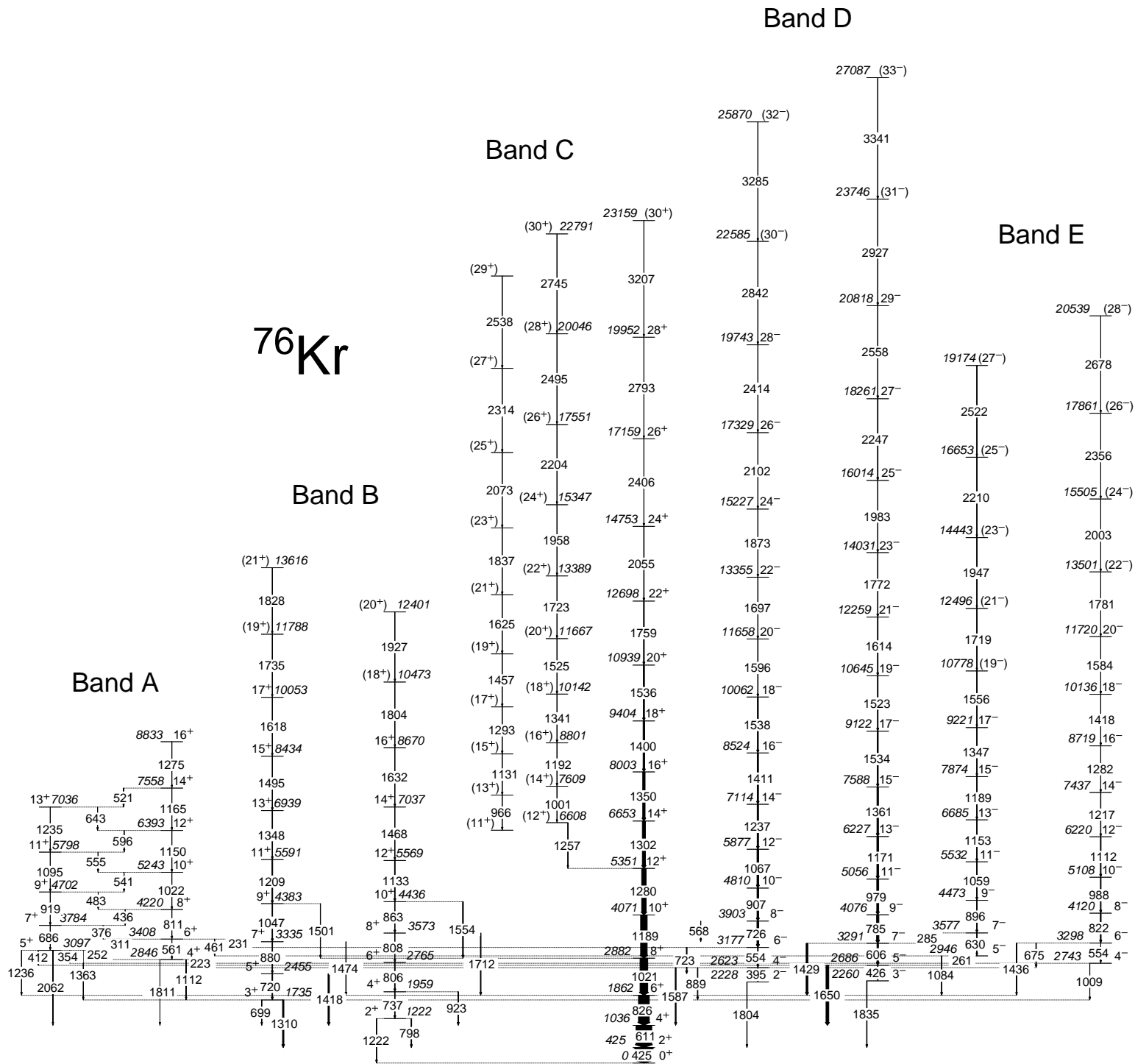
TABLE I: Spins, parities, energies, transition intensities and DCO ratios for the ground-state band of ^{76}Kr.

$_iI_n^\pi$	E_{lvl} (keV)	E_γ (keV)	I_γ	R_{DCO}	$\pm$	$_fI_n^\pi$
0_1^+	0	—	—	—	—	—
2_1^+	425	425	100	0.881	0.008	0_1^+
4_1^+	1036	611	87	1.000	0.011	2_1^+
6_1^+	1862	826	60	1.069	0.013	4_1^+
8_1^+	2882	1021	43	1.098	0.016	6_1^+
10_1^+	4071	1189	36	1.100	0.018	8_1^+
12_1^+	5351	1280	25	gate	—	10_1^+
14_1^+	6653	1302	17	1.06	0.02	12_1^+
16_1^+	8003	1350	13	1.00	0.03	14_1^+
18_1^+	9404	1400	8.8	0.99	0.04	16_1^+
20_1^+	10939	1536	6.3	1.10	0.04	18_1^+
22_1^+	12698	1759	4.3	1.13	0.07	20_1^+
24_1^+	14753	2055	2.6	1.09	0.08	22_1^+
26_1^+	17159	2406	1.2	1.11	0.13	24_1^+
28_1^+	19952	2793	0.5	1.06	0.28	26_1^+
(30_2^+)	23159	3207	0.1	—	—	28_1^+

TABLE II: Spins, parities, energies, transition intensities and DCO ratios for Band **A** of ^{76}Kr.

$_iI_n^\pi$	E_{lvl} (keV)	E_γ (keV)	I_γ	R_{DCO} [a]	$\pm$	$_fI_n^\pi$
4_3^+	2846	223	0.3	—	—	4_1^-
		1112	3.9	1.68	0.07	3_1^+
		1811	0.3	2.14	0.54	4_1^+
5_2^+	3097	252	1.5	1.02	0.07	4_3^+
		354	0.3	1.12	0.54	4_2^+
		412	0.8	2.17	0.22	5_1^-
		1236	0.8	1.79	0.31	6_1^+
		1363	0.2	—	—	3_1^+
		2062	1.0	1.51	0.22	4_1^+
6_3^+	3408	231	0.5	—	—	6_1^-
		311	1.6	0.97	0.04	5_2^+
		461	0.5	1.16	0.13	5_2^-
		561	0.9	1.71	0.26	4_3^+
7_2^+	3784	686	0.9	1.73	0.26	5_2^+
		376	1.5	1.02	0.05	6_3^+
8_3^+	4220	436	1.1	0.94	0.05	7_2^+
		811	1.0	2.26	0.19	6_3^+
9_2^+	4702	919	1.2	2.18	0.16	7_2^+
		483	0.7	0.77	0.06	8_3^+
10_3^+	5243	541	0.5	0.93	0.09	9_2^+
		1022	1.2	1.86	0.19	8_3^+
11_2^+	5798	1095	1.3	2.58	0.16	9_2^+
		555	0.5	1.21	0.14	10_3^+
12_3^+	6393	1150	1.2	2.37	0.20	10_3^+
		596	0.3	1.10	0.68	11_2^+
13_3^+	7036	1235	0.2	2.41	0.32	11_2^+
		643	0.5	1.07	0.14	12_3^+
14_3^+	7558	521	0.3	0.78	0.08	13_3^+
		1165	0.8	1.68	0.35	12_3^+
16_4^+	8833	1275	0.3	2.51	0.65	14_3^+

[a]Gates on 252, 311, 376 keV "dipole" transitions.

spin, assumed to have dominant stretched $M1$ character. With these gates, the other cross-over transitions give DCO ratios of $\sim$1.0, as do the ΔI=1 linking transitions to the negative-parity bands, which are assigned as pure stretched $E1$ transitions. Both the ΔI=2 in-band transitions and the ΔI=0 transitions linking to the negative parity bands have DCO ratios of $\sim$2.0, as expected for stretched electric quadrupole, and $I \rightarrow I$ electric dipole transitions, respectively. The ΔI=1 linking transitions to the positive-parity bands give intermediate DCO ratios, suggesting mixed $M1/E2$ character. Although a DCO ratio could not be reliably extracted for the weak ΔI=2, 1363-keV transition from the 3097-keV state of this Band **A** (assigned I^π=5$^+$) to the yrast 3$^+$ state. It should be noticed that the existence of this transition strongly supports the positive-parity assignment for Band **A**, as an $M2$ transition would not be expected to compete with the other linking transitions. Although the discussion in the following section will focus primarily on the properties of the bands observed in the high-spin region ($I \geq$18$\hbar$), we note that Tripathy *et al.* [26] have recently studied the structure of Band **A** using a deformed configuration-mixing shell model based on Hartree-Fock states. They predicted levels of 13_3^+ and 14_3^+ at approximately 7.0 and 7.5 MeV, respectively. The new levels identified here correspond extremely well with those predictions. As in the study by Döring *et al.* [9], this band is interpreted as a K=4$^+$ structure produced by a two-neutron excitation.

The 3$^+$, 5$^+$ and 7$^+$ states assigned to Band **B** have been observed in previous work [8]. We have identified seven additional states built upon this structure, establishing a rapid alignment of $\sim$3$\hbar$ in this band at a rotational frequency ω=0.40 MeV/$\hbar$. In previous work [8] the 2$^+$, 4$^+$ and 6$^+$ states in the even-spin sequence at 1222, 1959 and 2765 keV were interpreted in terms of a γ-vibrational structure [4], with the 8$^+$ and 10$^+$ states built upon this structure at 3573 and 4436 keV. We have confirmed these levels, and extended the band to I^π=20$^+$. In contrast to its odd-spin partner, no significant alignment process is observed in the even spin sequence.

Band **C** has been observed for the first time in the present study. Gamma-ray spectra for the two signatures of this band are shown in Figs. 1 b) and c), respectively, while the data for the band is presented in Table IV. This was the most weakly populated of the high-spin bands observed in the present work, and definite spin and parity assignments were therefore not possible. One signature of Band **C** is tentatively linked to the ground-state band by a single 1257-keV transition. Figure 4 a) shows the sum γ-ray spectrum obtained from a double coincidence gate set on this linking transition and the 1001 and 1192-keV transitions of Band **C**, meanwhile Fig. 4 b) shows the 1257-keV linking transition when a double coincidence gate is set on the two lowest transitions (1001 and 1192 keV) of Band **C**. All of the other transitions in Band **C**, as well as transitions in the ground-state band up to 1280-keV γ ray can be seen in this spectrum. The R_{DCO} ratio for the 1257-keV transition is consistent with

TABLE III: Spins, parities, energies, transition intensities and DCO ratios for Band **B** of ^{76}Kr.

$_iI_n^\pi$	E_{lvl} (keV)	E_γ (keV)	I_γ	R_{DCO}	$\pm$	$_fI_n^\pi$
2_2^+	1222	798	3.4	0.74	0.10	2_1^+
		1222	2.6	1.07	0.18	0_1^+
3_1^+	1735	699	1.4	—	—	4_1^+
		1310	7.7	0.71	0.06	2_1^+
4_2^+	1959	737	3.1	0.97	0.11	2_2^+
		923	3.8	0.67	0.08	4_1^+
5_1^+	2455	720	3.9	1.09	0.08	3_1^+
		1418	7.8	0.86	0.07	4_1^+
6_2^+	2765	806	3.3	1.00^a	0.05	4_2^+
7_1^+	3335	880	3.2	0.98	0.05	5_1^+
		1474	2.3	0.98	0.10	6_1^+
8_2^+	3573	808	2.1	1.00^a	0.05	6_2^+
		1712	4.0	1.05	0.09	6_1^+
9_1^+	4383	1047	3.3	gate	—	7_1^+
		1501	1.5	—	—	8_1^+
10_2^+	4436	863	2.5	gate	—	8_2^+
		1554	4.6	—	—	8_1^+
11_1^+	5591	1209	4.4	0.96	0.05	9_1^+
12_2^+	5569	1133	3.5	1.06	0.08	10_2^+
13_1^+	6939	1348	2.8	0.95	0.06	11_1^+
14_2^+	7037	1468	1.3	1.11	0.18	12_2^+
15_2^+	8434	1495	2.0	1.06	0.10	13_1^+
16_2^+	8670	1632	1.5	0.87	0.18	14_2^+
17_1^+	10053	1618	0.6	0.87	0.12	15_2^+
(18_3^+)	10473	1804	1.9	—	—	16_2^+
(19_2^+)	11788	1735	0.3	—	—	17_2^+
(20_3^+)	12401	1927	0.3	—	—	(18_3^+)
(21_2^+)	13616	1828	0.2	—	—	(19_2^+)

^{a}doublet

TABLE IV: Spins, parities, energies, transition intensities and DCO ratios for Band **C** of ^{76}Kr.

$_iI_n^\pi$	E_{lvl} (keV)	E_γ (keV)	I_γ	R_{DCO}	$\pm$	$_fI_n^\pi$
(12_4^+)	6608	1257	0.3	1.17	0.11	12_1^+
(13_3^+)	X+966	966	1.0	gate	—	(11_3^+)
(14_4^+)	7609	1001	0.4	gate	—	(12_4^+)
(15_2^+)	X+2097	1131	0.4	0.96	0.11	(13_3^+)
(16_3^+)	8801	1192	1.0	1.12	0.07	(14_4^+)
(17_1^+)	X+3390	1293	1.8	0.90	0.11	(15_2^+)
(18_2^+)	10142	1341	1.3	0.95	0.08	(16_4^+)
(19_1^+)	X+4847	1457	1.2	0.83	0.12	(17_1^+)
(20_2^+)	11667	1525	1.2	1.06	0.11	(18_2^+)
(21_1^+)	X+6472	1625	1.2	1.46	0.31	(19_1^+)
(22_2^+)	13389	1723	0.8	0.99	0.09	(20_2^+)
(23_1^+)	X+8309	1837	0.8	1.11	0.20	(21_1^+)
(24_2^+)	15347	1958	0.8	1.23	0.16	(22_2^+)
(25_1^+)	X+10382	2073	0.5	1.08	0.27	(23_1^+)
(26_2^+)	17551	2204	0.4	1.15	0.26	(24_2^+)
(27_1^+)	X+12696	2314	0.3	—	—	(25_1^+)
(28_2^+)	20046	2495	0.2	—	—	(26_2^+)
(29_1^+)	X+15234	2538	0.1	—	—	(27_1^+)
(30_1^+)	22791	2745	0.1	—	—	(28_2^+)
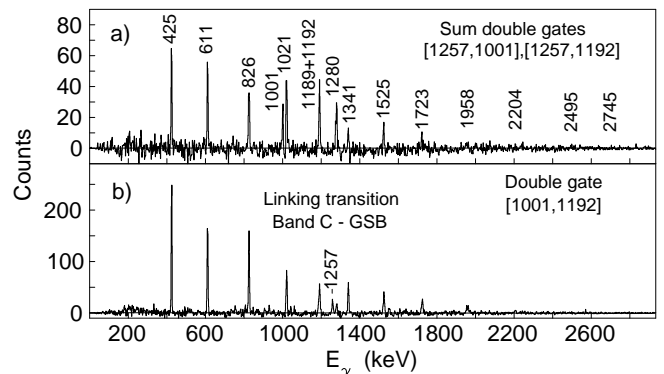
FIG. 4: Upper panel shows the sum of the background subtracted γ-ray spectrum in coincidence with a double gate set on the 1001 and 1192 keV transitions in Band **C** and the 1257 keV linking transition. Lower panel shows the background subtracted γ-ray spectrum in coincidence with a double gate set on the 1001 and the 1192 keV transitions in Band **C**. The 1257 keV transition links Band **C** and the ground-state band (GSB).

either an $\Delta I=2$ stretched quadrupole, or a $\Delta I=0$ non-stretched predominantly dipole transition. If the former is assigned, Band **C** would be yrast throughout the entire spin range over which it was observed in this experiment, and its very weak population relative to the ground-state band would then be difficult to understand. We therefore favour the latter choice and have tentatively assigned ($I^\pi=12^+$) to the 6608-keV state of this band, although this assignment must be considered uncertain at the $\pm 2\hbar$ level. For the signature partner, no linking transitions could be established. The tentative ($I^\pi=11^+$) assignment for the lowest observed state of this signature is based on the rigid rotational properties of the band, and the similarity of the moments of inertia for the two signatures under this assignment, see Fig. 7. The excitation energy of the odd-spin sequence is not determined experimentally, and the (11^+) state is arbitrarily positioned at 6.4 MeV excitation energy in Fig. 3, corresponding to a small signature splitting. With the above assignments, band **C** is near-yrast at high spins, but becomes rapidly non-yrast at low spins. This naturally accounts for the fragmentation of the decay out of this band at low spin that prevented its conclusive linking into the remainder of the ^{76}Kr level scheme.

Previous work [5] established the negative-parity Band **D** to a tentative spin of $22\hbar$. In that work, the transition from 19^- to 17^- was tentatively assigned as 1614 keV, while 1596 and 1697-keV transitions were proposed to extend the band from 18^- to 22^-. We have confirmed the 1596 and 1697-keV transitions in the even-spin sequence. The current data, however, indicate that a 1523-keV γ-ray (observed in Ref. [7] but assigned to the decay of the 17^- state) de-excites the 19^- state, and that the 1614-keV transition rather de-excites the 21^- state. As can be seen in Fig. 2 a), this band, which becomes yrast at high spins, was very strongly populated in the present

TABLE V: Spins, parities, energies, transition intensities and DCO ratios for Band **D** of ^{76}Kr.

$_iI_n^\pi$	E_{lvl} (keV)	E_γ (keV)	I_γ	R_{DCO}	±	$_fI_n^\pi$
2_1^-	2228	1804	0.3	0.51	0.13	2_1^+
3_1^-	2260	1835	2.7	0.79	0.10	2_1^+
4_1^-	2623	395	1.3	0.88	0.09	2_1^-
		889	3.0	0.69	0.05	3_1^+
		1587	5.0	0.79	0.09	4_1^+
5_1^-	2686	426	1.0	—	—	3_1^-
		1650	15.0	0.55	0.02	4_1^+
6_1^-	3177	554	3.8	0.94	0.03	4_1^-
		723	4.2	0.70	0.04	5_1^+
7_1^-	3291	606	8.5	0.97	0.02	5_1^-
		1429	10.0	0.57	0.01	6_1^+
8_1^-	3903	568	1.5	0.64	0.06	7_1^+
		726	10.1	0.87	0.02	6_1^-
9_1^-	4076	785	12.8	gate	—	7_1^-
10_1^-	4810	907	9.3	gate	—	8_1^-
11_1^-	5056	979	10.7	1.07	0.02	9_1^-
12_1^-	5877	1067	9.4	1.04	0.02	10_1^-
13_1^-	6227	1171	9.5	0.99	0.02	11_1^-
14_1^-	7114	1237	7.5	1.03	0.03	12_1^-
15_1^-	7588	1361	8.4	1.05	0.03	13_1^-
16_1^-	8524	1411	6.7	1.12	0.04	14_1^-
17_1^-	9122	1534	5.6	1.07	0.04	15_1^-
18_1^-	10062	1538	5.3	1.07	0.04	16_1^-
19_1^-	10645	1523	3.4	1.03	0.04	17_1^-
20_1^-	11658	1596	2.4	1.22	0.09	18_1^-
21_1^-	12259	1614	3.4	0.99	0.04	19_1^-
22_1^-	13355	1697	1.9	1.12	0.09	20_1^-
23_1^-	14031	1772	2.5	1.07	0.07	21_1^-
24_1^-	15227	1873	1.3	0.97	0.09	22_1^-
25_1^-	16014	1983	1.8	1.05	0.09	23_1^-
26_1^-	17329	2102	0.9	1.12	0.16	24_1^-
27_1^-	18261	2247	1.2	1.26	0.16	25_1^-
28_1^-	19743	2414	0.5	1.04	0.19	26_1^-
29_1^-	20818	2558	0.6	1.09	0.21	27_1^-
(30_1^-)	22585	2842	0.2	—	—	28_1^-
(31_1^-)	23746	2927	0.2	—	—	29_1^-
(32_1^-)	25870	3285	0.1	—	—	(30_1^-)
(33_1^-)	27087	3341	0.1	—	—	(31_1^-)

TABLE VI: Spins, parities, energies, transition intensities and DCO ratios for Band **E** of ^{76}Kr.

$_iI_n^\pi$	E_{lvl} (keV)	E_γ (keV)	I_γ	R_{DCO}	±	$_fI_n^\pi$
4_2^-	2743	1009	1.0	0.64	0.08	3_1^+
5_2^-	2946	261	1.2	0.99	0.07	5_1^-
		1084	3.1	0.55	0.04	6_1^+
6_2^-	3298	554	0.7	0.89	0.06	4_2^-
		675	2.9	0.81	0.04	4_1^-
		1436	1.8	0.95	0.07	6_1^+
7_2^-	3577	285	0.8	—	—	7_1^-
		630	1.7	gate	—	5_2^-
8_2^-	4120	822	4.8	1.04	0.04	6_2^-
9_2^-	4473	896	3.5	1.04	0.05	7_2^-
10_2^-	5108	988	3.9	gate	—	8_2^-
11_2^-	5532	1059	3.4	1.02	0.05	9_2^-
12_2^-	6220	1112	3.9	1.00	0.04	10_2^-
13_2^-	6685	1153	3.6	1.09	0.06	11_2^-
14_2^-	7437	1217	2.1	0.95	0.05	12_2^-
15_2^-	7874	1189	2.4	1.19	0.08	13_2^-
16_2^-	8719	1282	1.2	1.09	0.10	14_2^-
17_2^-	9221	1347	1.5	0.96	0.11	15_2^-
18_2^-	10136	1418	1.2	0.95	0.07	16_2^-
(19_2^-)	10778	1556	0.6	0.80	0.22	17_2^-
20_2^-	11720	1584	1.0	0.86	0.05	18_2^-
(21_2^-)	12496	1719	0.6	—	—	(19_2^-)
(22_2^-)	13501	1781	0.5	—	—	20_2^-
(23_2^-)	14443	1947	0.5	—	—	(21_2^-)
(24_2^-)	15505	2003	0.4	—	—	(22_2^-)
(25_2^-)	16653	2210	0.4	—	—	(23_2^-)
(26_2^-)	17861	2356	0.2	—	—	(24_2^-)
(27_2^-)	19174	2522	0.2	—	—	(25_2^-)
(28_2^-)	20539	2678	0.1	—	—	(26_2^-)

experiment. We have extended this band to $32\hbar$ and $33\hbar$ in the $\alpha=0$ and $\alpha=1$ signatures, respectively. The twelve new transitions are listed in Table V.

Band **E** was populated in this experiment with approximately one third the intensity of Band **D** at the equivalent spins. Previous work had established this structure to 13^- [8]. We agree with the previous assignments to this band, and extend the signatures to $27\hbar$ and $28\hbar$, respectively, delineating the full rotational alignment at $\omega=0.60$ MeV/$\hbar$ for the first time. The fifteen new transitions are detailed in Table VI.

In addition to the spectroscopic data presented above, the mean lifetimes of the high-spin states in the most strongly populated bands (ground-state band and Band **D**) were measured using the Doppler-shift attenuation method. Previous to this study no lifetimes of high-spin

states above spin $I^\pi=10^+$ for the ground-state band [5] and spin $I^\pi=13^-$ for Band **D** ($\alpha=1$) [6] were known. Figure 5 shows the experimental Doppler shifts, $F(\tau)$ values, (filled circles) for the transitions in the ground-state band as a function of γ-ray energy. The Doppler shifts were measured using the thin-target data, setting gates on the last three transitions at the top of the band. The side feeding into each of these states assumes a rotational band sequence, with 4 transitions. The quadrupole moment of the side feeding bands was chosen to be the same as in the band under consideration. Figure 5 a) shows fitted curves for three constant transition quadrupole moments along the band, corresponding to $Q_t=1.5$, 2.0 and 2.5 eb. The dash line represents the constant shift for decays that happen outside the thin target. This plot illustrates that a reasonable fit of the experimental data cannot be obtained if a constant Q_t is considered for the entire band. If a $Q_t=1.5$ eb is considered, the high-spin transitions are well described but a lower $F(\tau)$ value is predicted, for the lower spin transitions. The opposite occurs in the case that a $Q_t=2.0$ eb is considered. The lower spin states are well reproduced while the high-spin transitions are predicted to be faster (larger $F(\tau)$ values).

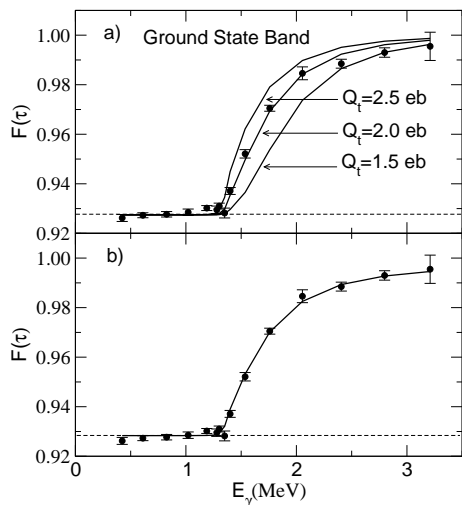To obtain a reasonable fit of the measured Doppler

FIG. 5: Experimental $F(\tau)$ values as a function of γ-ray energy for the ground-state band (filled circles) in ^{76}Kr. The solid lines in plot a) show the calculated $F(\tau)$ values for various constant transition quadrupole moments (Q_t=1.5, 2.0 and 2.5 eb). The solid line in plot b) shows the calculated $F(\tau)$ value, considering that Q_t varies as a function of spin (see text). The dashed line represents the $F(\tau)$ value reached by the recoils that leave the target.

shifts, the Q_t value was approximately modelled as $Q_t(I) = Q_t^{top} + \delta Q_t \sqrt{I^{top} - I}$. The *top* superscript indicates the highest-spin state observed experimentally in a band for the current work, for which a centroid shift could be measured. In the current data, this corresponds to a I^{top}=30$^+$, 31$^-$, 30$^-$ for the ground-state band, Band **D** (α=1) and Band **D** (α=0), respectively. The δQ_t represents the variation of the Q_t value within the band. The resulting fit is shown in Fig. 5 b).

For the lower-spin states, the backed-target data was used to determine the lifetimes. The spectra were obtained gating on transitions above the level of interest. The side feeding that contributes to the lifetime of the states of interest was modeled using a cascade of four transitions of adjustable lifetime. Figure 6 shows the fit to the lineshape of the 1189-keV transition of the ground-state band. The lifetimes of the lowest spin states could not be determined since a large fraction of the decays took place when the recoil was completely stopped, therefore the transitions show a sharp peak, lacking any shape that could be used to determine the lifetime. Table VII summarizes the measured Q_t for the ground-state band and Band **D**.

IV. DISCUSSION

The kinematic $\Im^{(1)}$ and dynamic $\Im^{(2)}$ moments of inertia for the positive-parity bands in ^{76}Kr observed to high spin are shown in Fig. 7, while for the negative-parity bands are shown in Fig. 8 and Fig. 9. For the
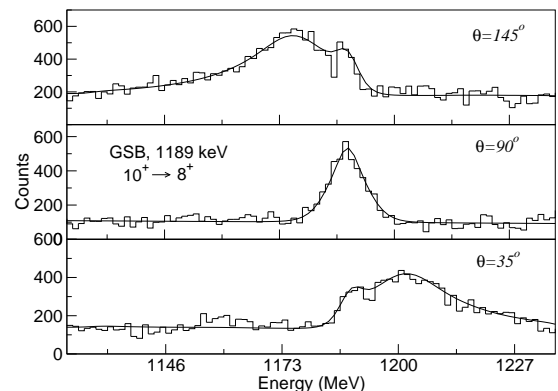

FIG. 6: Lineshape fit in ^{76}Kr for the ground-state band transition, 1189 keV, from the backed-target data. The top, middle and bottom panel correspond to lineshapes at the mean angles 145°, 90° and 35° respectively.
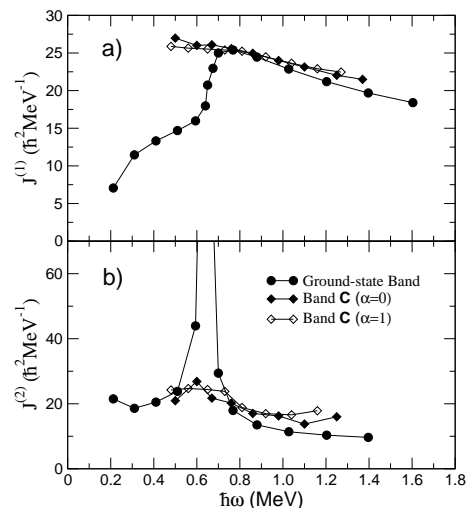

FIG. 7: a) Kinematic and b) dynamic moments of inertia for the ground-state band and Band **C** in ^{76}Kr plotted versus rotational frequency.

ground-state band and the negative-parity bands **D** and **E**, sharp rotational alignments were observed at ,rotational frequencies of ω=0.65, 0.75, and 0.60 MeV/$\hbar$, respectively. As mentioned in the Introduction, these alignments have been previously interpreted [5, 8] as the simultaneous alignment of $g_{9/2}$ protons and neutrons in the ground-state band, the alignment of $g_{9/2}$ neutrons in the two quasi-proton excited configuration of Band **D**, and the alignment of $g_{9/2}$ protons in the two quasi-neutron excited configuration of Band **E**. Here we focus on the high-spin properties of the bands, and the interpretation of the newly identified Band **C**. First we note that all of the observed bands exhibit a gradual decrease in kinematic moment of inertia at the highest rotational fre-

TABLE VII: Transition quadrupole moments Q_t for the ground-state band and the Band **D** in ^{76}Kr, deduced from the current data, as a function of spin.

$_iI^\pi_n$	E_γ(keV)	Q_t (eb)	$_fI^\pi_n$
Band GSB			
30^+_2	3207	1.80 ± 0.10	28^+_1
28^+_1	2793	2.00 ± 0.10	26^+_1
26^+_1	2406	2.08 ± 0.10	24^+_1
24^+_1	2055	2.15 ± 0.10	22^+_1
22^+_1	1759	2.20 ± 0.10	20^+_1
20^+_1	1536	2.25 ± 0.10	18^+_1
18^+_1	1400	2.29 ± 0.10	16^+_1
16^+_1	1350	—	14^+_1
14^+_1	1302	—	12^+_1
12^+_1	1280	—	10^+_1
10^+_1	1189	$2.66^{+0.15}_{-0.09}$	8^+_1
8^+_1	1021	$2.77^{+0.02}_{-0.15}$	6^+_1
6^+_1	825	$2.81^{+0.06}_{-0.10}$	4^+_1
Band D $\alpha=1$			
31^-_1	2927	2.20 ± 0.10	29^-_1
29^-_1	2558	2.45 ± 0.10	27^-_1
27^-_1	2247	2.55 ± 0.10	25^-_1
25^-_1	1983	2.63 ± 0.10	23^-_1
23^-_1	1772	2.70 ± 0.10	21^-_1
21^-_1	1614	2.76 ± 0.10	19^-_1
19^-_1	1523	2.81 ± 0.10	17^-_1
17^-_1	1534	2.86 ± 0.10	15^-_1
15^-_1	1361	—	13^-_1
13^-_1	1171	—	11^-_1
11^-_1	979	$3.95^{+0.21}_{-0.10}$	9^-_1
9^-_1	785	$3.54^{+0.14}_{-0.11}$	7^-_1
Band D $\alpha=0$			
30^-_1	2842	1.80 ± 0.10	28^-_1
28^-_1	2414	2.10 ± 0.10	26^-_1
26^-_1	2102	2.22 ± 0.10	24^-_1
24^-_1	1873	2.32 ± 0.10	22^-_1
22^-_1	1697	2.40 ± 0.10	20^-_1
20^-_1	1596	2.47 ± 0.10	18^-_1
18^-_1	1538	2.54 ± 0.10	16^-_1
16^-_1	1411	2.59 ± 0.10	14^-_1
14^-_1	1237	—	12^-_1
12^-_1	1067	$5.34^{+0.28}_{-0.44}$	10^-_1
10^-_1	907	$3.48^{+0.17}_{-0.13}$	8^-_1

FIG. 8: a) Kinematic and b) dynamic moments of inertia for Band **D** in ^{76}Kr plotted versus rotational frequency.

FIG. 9: a) Kinematic and b) dynamic moments of inertia for Band **E** in ^{76}Kr plotted versus rotational frequency.

quencies, a characteristic feature of the increasing energy cost to build angular momentum as a band approaches termination and exhausts the spin content of its single-particle configuration [27]. With the exception of this gentle decrease at high rotational frequency, however, the constancy of the moment of inertia of Band **C** is remarkable. In contrast to the other bands, no rotational alignment process is evident in the ω=0.5–1.4 MeV/$\hbar$ frequency range over which Band **C** is observed. For Band **D**, the large kinematic moment of inertia at low spins has been interpreted [5, 7] in terms of a drastic reduction in pairing correlations in this configuration due to the blocking of the $[431]\frac{3}{2}^+$ and $[312]\frac{3}{2}^-$ proton orbitals and the low level density in the vicinity of the large shell gap a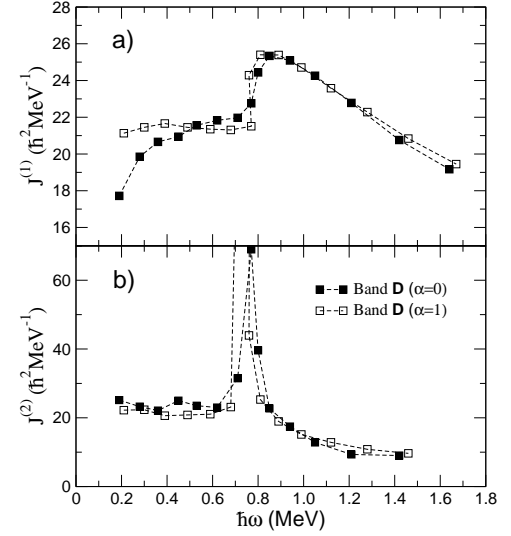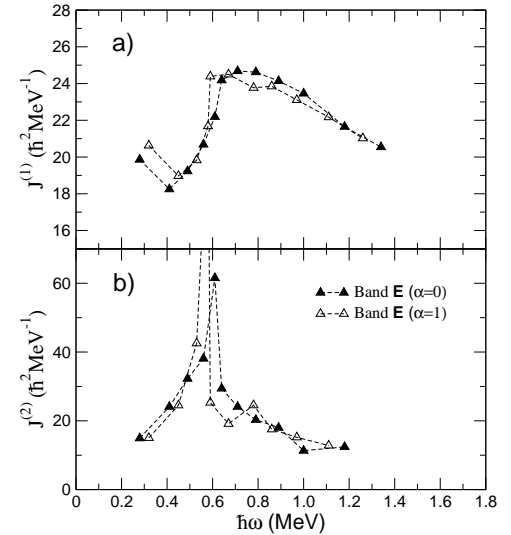t N, Z=38 for prolate deformations (see Fig. 1 in Ref. [3]). A modified argument, involving the blocking of the $[301]\frac{3}{2}^-$ and $[422]\frac{5}{2}^+$ neutron orbitals, applies to Band **E**. For Band **C**, the very large kinematic moment of inertia at low spin, its constancy with rotational frequency, and the absence of any alignment process, suggest a complete collapse of static pairing correlations and an even more dramatic example of rigid rotational behavior. The measured transition quadrupole moments of the ground-state band and the negative-parity Band **D** show a clear evolution with spin, see Fig. 12 a). It can be noted that the Q_t value decreases slightly after the band crossing and from there onwards a continuous decrease is observed as the highest spins are approached. This trend in the Q_t value at high spin states indicates that band
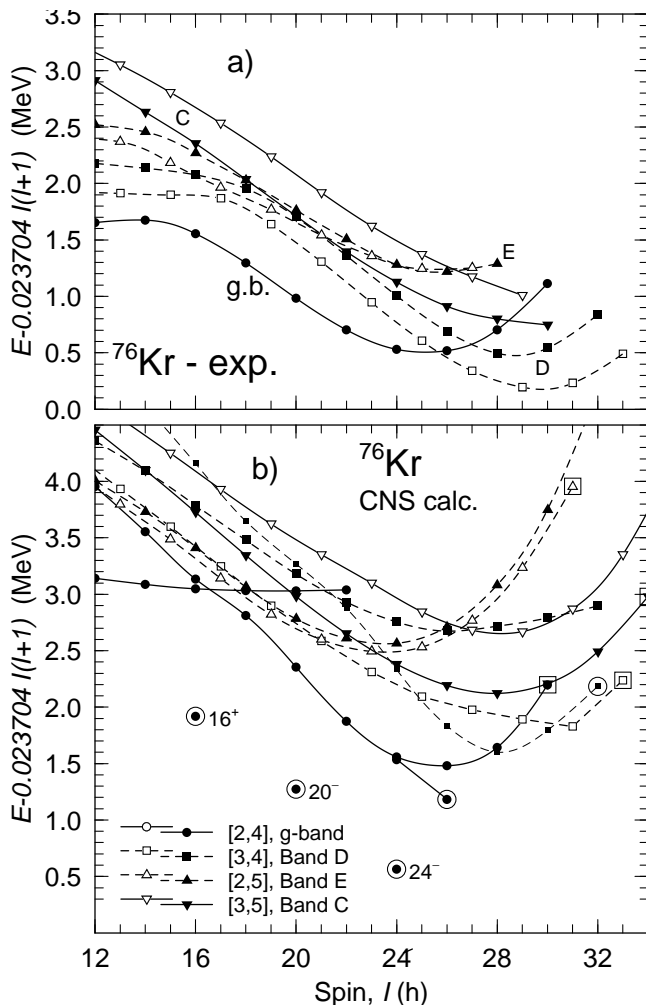
FIG. 10: Energies of high-spin collective configurations in ^{76}Kr relative to an $I(I + 1)$ reference plotted versus spin, from a) experiment, and b) configuration-dependent cranked Nilsson Strutinsky calculations. Solid (dashed) lines represent positive (negative) parity, and closed (open) symbols denote signature $\alpha=0$ ($\alpha=1$). In panel b) terminating states are encircled, while the maximum spin states which do not terminate are indicated by large squares. The calculated bands are labelled by $[p, n]$, where p (n) is the number of $g_{9/2}$ protons (neutrons). The band label has been added next to the assigned configuration. A second even spin [3,4] configuration lower in energy for the spin range $I\approx25$–30 is shown by a thinner line and smaller closed squares. Note that the absolute normalization for experiment and calculations is different

termination is approached [27], corroborating the gradual decrease in kinematic moment of inertia. A similar behaviour of the Q_t value along the ground-state band of ^{74}Kr has been observed previously [28]. Algora et $al.$ [28] argued that the main contributions for the change of Q_t at the band crossing is due to: i) the aligning particles originating from the $g_{9/2}$ orbital that contribute less to the quadrupole moment and ii) a shape-driving factor related to the angular momentum gain in the alignment process.
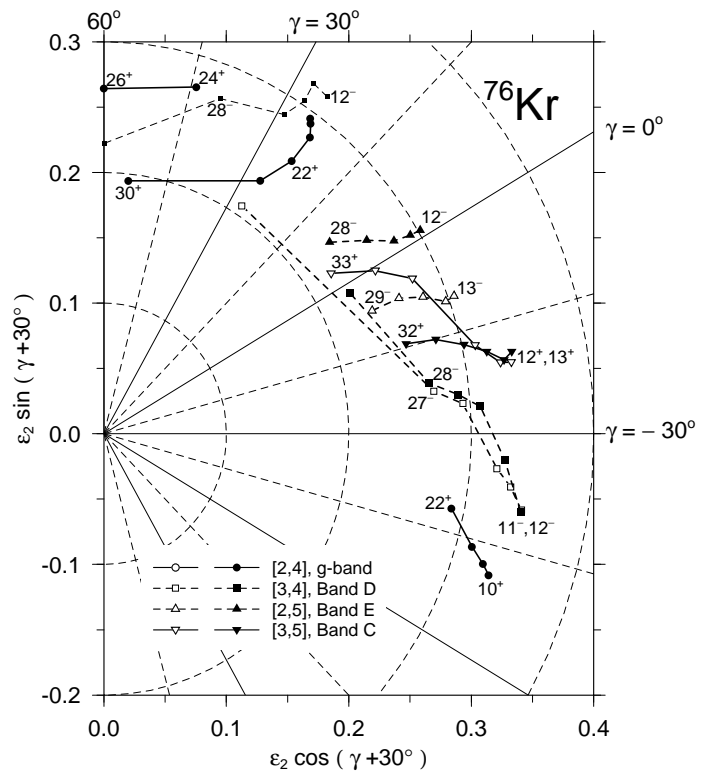

FIG. 11: Calculated deformation trajectories for ^{76}Kr. The deformations are shown for each fourth spin value except for the band terminating at $I^{\pi}=26^+$ where also the $I^{\pi}=24^+$ state is shown.

In order to gain further insight into the structure of the high-spin bands observed in ^{76}Kr, we have performed a theoretical analysis employing the configuration-dependent shell-correction approach with the cranked Nilsson potential [12, 13]. Pairing correlations were not included in these calculations, which can therefore only be compared to the experimental data in the high-spin regime ($I \geq 15\hbar$). The energies of the favoured high-spin collective configurations from these calculations are compared with the experimental results in Fig. 10. The theoretical bands are labelled by $[p, n]$, where p (n) represents the number of $g_{9/2}$ proton (neutron) orbitals occupied. The maximal spin values have been calculated assuming that the $p_{\frac{1}{2}}$ orbitals are empty, while the $f_{\frac{7}{2}}$ orbitals are fully occupied. The positive-parity ground-state band has configuration [2,4] in this notation, where the calculated deformation for the spin range $I=10$–$20\hbar$ is $\epsilon=0.25$–0.30 and $\gamma=20°$–25°. As indicated by the open square in Fig. 10 b), the 30^+ is a maximum spin state which effectively terminates the [2,4] configuration. The maximum spin 30^+ state is built as a $\pi\{[(g_{\frac{9}{2}})^2]_8[(f_{\frac{5}{2}},p_{\frac{3}{2}})^6]_6\}_{14} \otimes \nu\{[(g_{\frac{9}{2}})^4]_{12}[(f_{\frac{5}{2}},p_{\frac{3}{2}})^8]_4\}_{16}$ configuration, where subscripts outside brackets describe the angular momentum contributed by all of the particles outside the $N=Z=28$ ^{56}Ni core. This conclusion is reinforced, as can be seen in Fig. 11, by the cal-

culated evolution of the equilibrium nuclear shape for the [2,4] configuration, which evolves from prolate at low spins, through triaxial shapes to a close-to-oblate (γ=55°) I^π=30$^+$ state, showing still some collectivity at its maximum spin state. Comparing Figs. 10 a) and b), excellent agreement is found between the observed properties of the ground-state band and the calculations for the [2,4] configuration in the high-spin (I∼16–30$\hbar$) region, and the assigned 3207-keV transition at the top of this band can be considered as the observation of its high-spin termination. Nevertheless it can be noted that for spins up to I=16$\hbar$, a more energetically favoured band is calculated, presenting a large negative γ value. The calculations predict in addition two non-collective oblate states, for the [2,4] configuration at lower energy, namely at I^π=16$^+$ and 26$^+$ (see Fig. 10 b), open circles). For the I^π=26$^+$ state the spin is built from the $\pi\{[(g_\frac{9}{2})^2]_8[(f_\frac{5}{2},p_\frac{3}{2})^6]_4\}_{12} \otimes \nu\{[(g_\frac{9}{2})^4]_{12}[(f_\frac{5}{2},p_\frac{3}{2})^8]_2\}_{14}$ configuration.

In agreement with previous studies [5, 6, 7], the favoured negative-parity configuration, [3,4] in our notation, involves a proton excitation and the occupation of an additional proton $g_{9/2}$ orbital relative to the ground-state band. As can be seen in Fig. 10, the observed high-spin properties of Band **D** compare very favourably with the calculated spin-dependence of this configuration. The deformation for both signature partners is very similar. It evolves from γ=-40° up to large positive γ values in the spin range I∼11–33$\hbar$ but band termination is not predicted in either case at their maximum spins, see Fig. 11. Signature splitting at the highest spins is observed to be somewhat smaller in experiment than predicted by theory. The calculations predict at a deformation of ϵ=0.25–0.30 and γ=30–60° an energetically favoured band for the spin range I=22–32$\hbar$, that terminates at I_{max}=32 and presents a $\pi\{[(g_\frac{9}{2})^3]_{10.5}[(f_\frac{5}{2},p_\frac{3}{2})^5]_{5.5}\}_{16} \otimes \nu\{[(g_\frac{9}{2})^4]_{12}[(f_\frac{5}{2},p_\frac{3}{2})^6]_4\}_{16}$ configuration.

The next favoured negative-parity configuration is labelled [2,5] and involves a neutron excitation, with the occupation of an additional neutron $g_{9/2}$ orbital relative to the ground-state band. This configuration corresponds to that assigned to Band **E** by Döring *et al.* [8], and Fig. 10 shows a good agreement between the high-spin experimental data for Band **E** and the CNS calculations for the [2,5] configuration. Nevertheless it can be observed in Fig. 10, that the calculated curves for the [2,5] configuration show an energy increase at I≈23$\hbar$, while no real increase is observed in the experimental curves up to the highest observed spin values I=28$\hbar$. A possible explanation for this disagreement might be related to the appearance of a band crossing at high spins. Configurations with holes in $f_{7/2}$ might become competitive in energy at high spins, although with the current parameters that have been used in these calculations, these configurations lie higher in energy. A much more energetically favoured configuration that could cross the [2,5] configuration at high spin is an excited [3,4] band, but

in this case a non-smooth crossing, as it is observed experimentally, is expected when crossing the [2,5] and the [3,4] configuration. The calculations do not predict band termination at its highest spin values I_{max}=31, 32$\hbar$. Instead the deformation for this band stays in the range γ=-15–30°. It can be noted, particularly, the near signature degeneracy for the band at high spin in both theory and experiment.

The collective bands which appear lowest in energy in the CNS calculations after those discussed above have the positive-parity configuration [3,5], and can be considered as the combination of the proton and neutron excitations involved in Bands **D** and **E**, respectively. The favoured band has a signature α=0, *i.e.* even spin states. Two α=1 bands of similar energy are then calculated, depending on the chosen signature for the protons or neutrons, only one of the bands is drawn in Figs. 10 11. Although the spins of the experimentally observed states in Band **C** have not been definitively established, the two signatures of this band are plotted in Fig. 10 a) with the tentatively assigned spin values discussed in the previous section. With these spin assignments, excellent agreement between the properties of Band **C** and the calculations for the lowest pair of signatures for the [3,5] configuration is observed. The uncertain excitation energy of the odd-spin sequence simply corresponds to a vertical shift of this signature in Fig. 10 a). Calculations predict, as in the case of Band **E**, a collective behaviour for the highest spin values I_{max}=34, 35$\hbar$. The assignment of the [3,5] configuration to Band **C** also provides a natural explanation of the very rigid rotational properties for this band shown in Fig. 7. In the negative-parity Bands **D** and **E**, significant reductions in pairing correlations are associated with the blocking of proton orbitals just below and neutron orbitals just above the N, Z=38 prolate shell gap, respectively. In the [3,5] configuration, both of these proton and neutron orbitals are blocked. Combined with the already low-level densities at the proton and neutron Fermi surfaces for ^{76}Kr due to the large gap in the single-particle energy levels at N, Z=38, this blocking could lead to a complete collapse of static pairing correlations already at low spin values and the remarkably rigid rotational behavior of this band. As can be seen in Fig. 10 a), Band **C** is close to yrast at the highest spins observed here. At low spins, however, pairing correlations begin to favour the other bands and Band **C** becomes highly non-yrast, decaying out, presumably through fragmented pathways, in the I∼10$\hbar$ region. Together, these properties support the tentative spin assignments for Band **C** given in Fig. 3, and provide a consistent interpretation of the structure of this band based on the [3,5] configuration involving both proton and neutron excitations relative to the ground-state band.

It has been shown that, while the CNS calculations presented in Fig. 10 provide a good description of the angular-momentum dependence of the energies of the experimentally observed bands at high spin, the relative energies of the various configurations reveal a system-
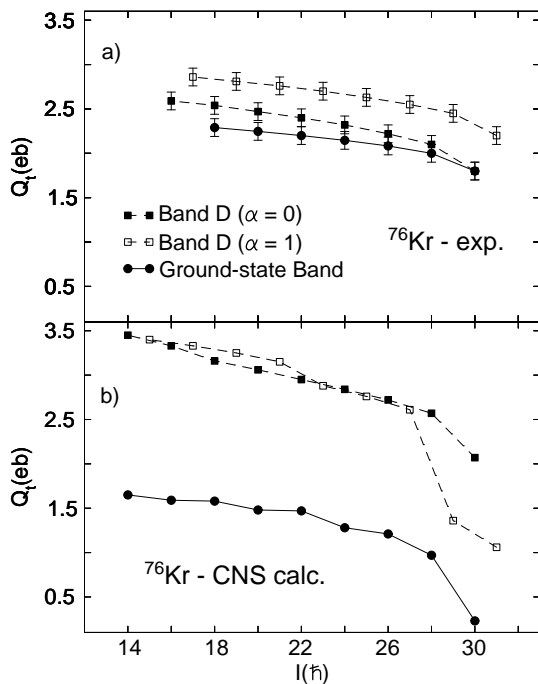
FIG. 12: Top panel shows the measured transition quadrupole moments Q_t for the ground-state band and Band **D**. Lower panel shows the calculated Q_t values for the [2,4] and [3,4] configurations which are interpreted as the ground-state band and Band **D**, respectively.

atic trend in which configurations with more $g_{9/2}$ orbitals occupied appear lower in energy in experiment than in theory. A clear example of this behaviour can be seen when comparing the ground-state band and Band **D**. The agreement between theory and experiment at high spins in the case of Band **D**, [3,4] configuration, could be improved if the [3,4] configuration was lowered relative to the ground-state band, [2,4] configuration, and this could be achieved by lowering the $g_{9/2}$ proton shell by approximately 0.5 MeV. The situation for the other observed bands is not so clear but it appears that if the neutron $g_{9/2}$ shell was also lowered by the same energy, the bands with many $g_{9/2}$ particles would be calculated too low in energy. Similar observations regarding the energetics of occupying the $g_{9/2}$ orbital have been made for a number of highly and superdeformed bands in the $A{\sim}60$ mass region [29, 30]. Together with these observations, the present data on ^{76}Kr provides additional support for a number of recent studies [31, 32, 33] in which it was concluded that the $g_{9/2}$ single-particle energy in this mass region is systematically placed too high relative to the pf-shell orbitals in all of the standard parameterizations.

Finally, Fig. 12 provides a comparison between the experimental transition quadrupole moment Q_t and the theoretical Q_t values for the high spin states of the ground-state band and Band **D** as a function of spin. In the case of the ground-state band the Q_t value decreases from $\sim$2.3 eb to 1.8 eb. For Band **D**, the decrease

is larger and changes from $\sim$2.8 eb to 2.2 eb (α=1) and from $\sim$2.5 eb to 1.8 eb (α=0). A similar trend of the Q_t value as a function of spin has been previously observed, for terminating bands, in other mass regions, $A{\sim}110$ [34], $A{\sim}60$ [35]. The CNS calculations performed to obtain the Q_t values are known to present some problems when calculating transition probabilities, and therefore the calculated Q_t values have to be treated with some caution when the band termination is approached [13, 27]. Keeping in mind the limitation in the calculations of the Q_t values at high spin states, can still be observed the general features of the Q_t values as we go higher in spin. Both experimental and theoretical Q_t values show a smooth drop as the band loses collectivity. The calculations yield Q_t values that are generally larger at large negative γ deformation but smaller when the bands approach termination at large positive γ deformation.

V. SUMMARY

In summary, high-spin states in ^{76}Kr have been studied in the fusion-evaporation reaction ^{40}Ca(^{40}Ca,4p)^{76}Kr using GAMMASPHERE and the MICROBALL multi-detector arrays. The yrast band and two previously observed negative-parity bands in ^{76}Kr have been extended to $I{\sim}30\hbar$, and their lifetimes measured using the Doppler shift attenuation method. A new pair of signature partner bands have been identified with remarkably rigid rotational behavior. The high-spin properties of these bands were studied within the framework of configuration-dependent cranked Nilsson-Strutinsky calculations without pairing. Previous configuration assignments for the ground-state and negative-parity bands were confirmed, and a consistent interpretation of the new band was achieved based on a configuration in which 3 $g_{9/2}$ proton orbitals and 5 $g_{9/2}$ neutron orbitals are occupied, i.e. involving both proton and neutron excitations relative to the ground-state band. The calculated transition quadrupole moments for the ground-state band and Band **D** present some differences with the experimental measured values in absolute scale, nevertheless both show a smooth decrease as band termination is approached.

[1] R. B. Piercey et al., Phys. Rev. Lett **47**, 1514 (1981).

[2] R. Bengtsson, P. Möller, J. R. Nix, and J. Zhang, Phys. Scr. **29**, 402 (1984).

[3] W. Nazarewicz, J. Dudek, R. Bengtsson, T. Bengtsson, and I. Ragnarsson, Nucl. Phys. **A435**, 397 (1985).

[4] D. Galeriu, D. Bucurescu, and M. Ivascu, J. Phys. G **12**, 329 (1986).

[5] C. J. Gross, J. Heese, K. P. Lieb, S. Ulbig, W. Nazarewicz, C. J. Lister, B. J. Varley, J. Billowes, A. A. Chishti, J. H. McNeill, et al., Nucl. Phys. **A501**, 367 (1989).

[6] R. B. Piercey, A. V. Ramayya, J. H. Hamilton, X.-J. Sun, Z. Z. Zhao, R. L. Robinson, H. J. Kim, and J. C. Wells, Phys. Rev. C **25**, 1941 (1982).

[7] M. S. Kaplan, J. X. Saladin, L. Faro, D. F. Winchell, H. Takai, and C. N. Knott, Phys. Lett. B **215**, 251 (1988).

[8] J. Döring, G. D. Johns, R. A. Kaye, M. A. Riley, S. L. Tabor, P. C. Womble, and J. X. Saladin, Phys. Rev. C **52**, R2284 (1995).

[9] J. Döring, G. D. Johns, R. A. Kaye, M. A. Riley, S. Tabor, and J. X. Saladin, Phys. Lett. B **381**, 40 (1996).

[10] B. Wörmann, K. P. Lieb, R. Diller, L. Lühmann, J. Keinonen, L. Cleemann, and J. Eberth, Nucl. Instrum. Methods Phys. Res. A **431**, 170 (1984).

[11] B. Cederwall, Nucl. Instrum. Methods Phys. Res. A **354**, 591 (1995).

[12] T. Bengtsson and I. Ragnarsson, Nucl. Phys. **A436**, 14 (1985).

[13] A. V. Afanasjev and I. Ragnarsson, Nucl. Phys. **A591**, 387 (1995).

[14] I.-Y. Lee, Nucl. Phys. **A520**, 641c (1990).

[15] D. G. Sarantites, P. F. Hua, M. Devlin, L. G. Sobotka, J. Elson, J. T. Hood, D. R. LaFosse, J. E. Sarantites, and M. R. Maier, Nucl. Instrum. Methods Phys. Res. A **381**, 418 (1996).

[16] C. E. Svensson et al., Nucl. Instrum. Methods Phys. Res. A **396**, 228 (1997).

[17] D. Seweryniak, J. Nyberg, C. Fahlander, and A. Johnson, Nucl. Instrum. Methods Phys. Res. A **340**, 353 (1994).

[18] D. C. Radford, Nucl. Instrum. Methods Phys. Res. A **361**, 297 (1995).

[19] D. Ward et al., Nucl. Phys. **A529**, 315 (1991).

[20] J. F. Ziegler, http://www.srim.org.

[21] C. E. Svensson et al., Acta Phys. Pol. **B9**, 2413 (2001).

[22] C. J. Chiara, D. R. LaFosse, D. G. Sarantites, M. Devlin, F. Lerma, and W. Reviol, Nucl. Instrum. Methods Phys. Res. A **523**, 374 (2004).

[23] J. J. Valiente-Dobón et al., Acta Phys. Pol. B (to be published).

[24] J. C. Wells and N. R. Johnson, ORNL Physics Division Progress Report for period ending September 30 **No. ORNL-6689** (1991).

[25] J. F. Ziegler and W. K. Chu, At. Data Nucl. Data Tables **13**, 463 (1974).

[26] K. C. Tripathy and R. Sahu, J. Phys. G **26**, 1271 (2000).

[27] A. V. Afanasjev, D. B. Fossan, G. J. Lane, and I. Ragnarsson, Phys. Rep. **322**, 1 (1999).

[28] A. Algora et al., Phys. Rev. C **61**, 031303R (2000).

[29] C. E. Svensson et al., Phys. Rev. Lett. **79**, 1233 (1997).

[30] D. Ward et al., Phys. Rev. C **63**, 014301 (2001).

[31] H. Madokoro and M. Matsuzaki, Prog. Theor. Phys. **101**, 1027 (1999).

[32] A. V. Afanasjev, I. Ragnarsson, and P. Ring, Phys. Rev. C **59**, 3166 (1999).

[33] Y. Sun, J. Zhang, M. Guidry, J. Meng, and S. Im, Phys. Rev. C **62**, 021601 (2000).

[34] R. Wadsworth et al., Phys. Rev. Lett. **80**, 1174 (1998).

[35] C. E. Svensson et al., Phys. Rev. Lett. **80**, 2558 (1998).